The transverse compression of PPTA fibers

Part I   *Single fiber transverse compression testing*

J. SINGLETARY, H. DAVIS*
College of Textiles, North Carolina State University, Box 8301, Raleigh, North Carolina, USA 27695-8301
E-mail: hdavis@tx.ncsu.edu

M. K. RAMASUBRAMANIAN
College of Wood and Paper Science, North Carolina State University, Raleigh, North Carolina, USA

W. KNOFF
DuPont de Nemours and Co., Inc., Advanced Fibers Systems, Richmond, Virginia, USA

M. TONEY
Albany International Research Co., Mansfield, Massachusetts, USA

We report on the transverse compression testing of fine, highly anisotropic polymer fibers. Single KEVLAR 29 fibers were laid on a flat, stiff platen, and compressed by a second, stiff, parallel platen. Test output was a force-deflection curve, from which the effective transverse modulus, apparent strain at yield and the work required to compress the fibers were determined. The effects of specimen aspect ratio was examined experimentally and by finite element simulation for loaded fiber lengths of 1/4 to 7 fiber diameters, and a method proposed to deduce the plane strain response from short aspect ratio tests.
© *2000 Kluwer Academic Publishers*

1. Introduction

While the axial properties of poly(*para*-phenyleneterepthalamide) (PPTA) and other, highly-oriented fibers have been extensively researched, their transverse properties have received comparatively little attention. Many applications of highly-oriented fibers require understanding of their behavior in transverse compression, such as ballistic or cut-resistant cloth [1], the bearing strength of composites or clamping strength of cloth, the compaction of nonwovens [2], the tribology of fiber-reinforced friction materials, hydrostatic pressure in underwater cables [3], and composites micromechanics models [4, pages 134–137].

This paper presents test results and simulation of the single fiber transverse compression test (SFTCT), using a novel test device. In SFTCT, a fiber is laid flat on a stiff platen and pressed by a second, parallel, stiff platen (Fig. 1). Analogous tests have been applied previously to various cylindrical test specimens, including concrete cylinders (e.g. [5, 6]) and ceramic fibers [7–9], where it is called the *Brazilian Test*. SFTCT presents three experimental difficulties when testing fine, polymer fibers:

1. Their small diameter and low modulus make test specimens very compliant per unit length.
2. The test requires accurate measurement of platen travel, because commercial, highly-oriented polymer fibers deform elastically only for the first 0.5–1 μm of platen travel after initial contact [1, 10–12].

3. During this initial, elastic contact, the fiber stress state is sensitive to the geometry of the contact patches between fiber and platens [1], which is itself sensitive to surface roughness [12, 13], variations in fiber diameter and asperities on the fiber surface [14].

To ameliorate these experimental difficulties, investigators have tested thick monofilaments [14–19], compressed multiple fibers simultaneously [1, 20], or compressed long lengths of fibers $(20 < L/D < 100)$ [10–12] (for detailed reviews, see [12, 21]). All these alternatives present additional difficulties. The cross-sectional structure of thick monofilaments strongly influences their transverse deformation [18], and probably differs from the cross-section of fine, commercial fibers. Compressing multiple fibers initially compresses only the tallest fibers, and may compress these past yield before contacting shorter fibers. This would result in spuriously low estimated fiber elastic stiffness when normalized by the total length of fiber compressed. Indeed, such studies [1] have reported lower transverse stiffnesses than single fiber tests [10, 12]. Pressing long lengths of single fibers appears the best of these three alternatives, but places high demands on platen parallelism, to avoid incomplete initial contact as above, and may not accurately simulate the stress

---

* Author to whom all correspondence should be addressed.
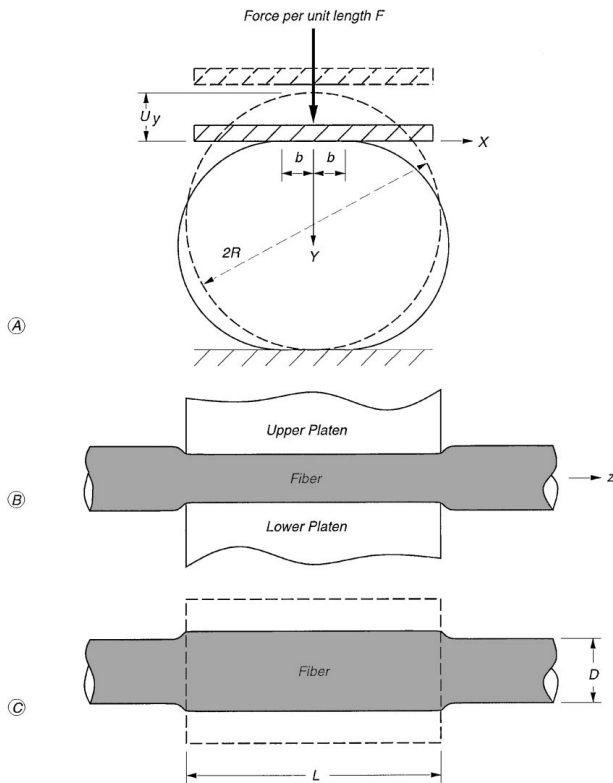
Figure 1 Load conditions of single fiber transverse compression test (SFTCT), showing variables used in this study. (A): Cross-section, (B): side view, (C): top view.

state of fibers compressed along short lengths, such as neighboring fibers or knife-edge contact.

It is appropriate to assume the steel, glass, or ceramic platens used are rigid relative to typical polymers, leading to a classical, Hertzian contact mechanics problem of the plane strain compression of a right circular cylinder between rigid, parallel platens (e.g. [22–24]). The solution to this problem has been extended to transversely isotropic cylinders [1, 19] to account for fiber orientation. Other analyses have been suggested, based on series expansions of the boundary loads, but they either do not lead to solutions which are easily amenable to fitting to experimental data, or do not incorporate the contact problem's geometric nonlinearity [25–27].

In this paper, we introduce a novel test device, capable of SFTCT of fine, polymer fibers at $1/4 < L/D < 7$. We verify the test device by comparing results on KEVLAR 29 to the literature. We then examine the effects of aspect ratio, L/D, with experiment and finite element (FE) simulation, and present a method to extract the plane strain transverse modulus from test at short fiber lengths.

2. Theory
2.1. Elastic transverse compression
Two analyses have been presented for transversely isotropic fibers, which are based on the Hertzian contact problem of an isotropic cylinder compressed between two rigid, parallel platens. Phoenix and Skelton [1] modeled contact between both the upper and lower platens as distributed, Hertzian contact loads (Fig. 2A), and determined the stress distribution along $[x = 0, 0 < y < 2R, z]$. Jawad and Ward [19] assumed the upper
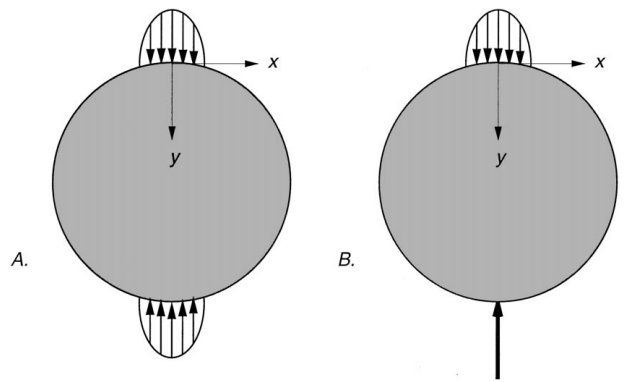
Figure 2 Boundary conditions of SFTCT analyses: (A) Phoenix and Skelton (1974). (B) Jawad and Ward (1978).

load was distributed, but the lower load was a line load (Fig. 2B), and determined the stress distribution across $[x = 0, 0 < y < R, z]$, arguing that the lower stress distribution was a mirror image in the actual fiber. Both models predict essentially identical stress distributions [21], therefore, following Jones *et al.* [12], we focus on the Jawad and Ward model, whose resulting equations are simpler to fit to experimental data. Jawad and Ward use the contact patch width $2b(F)$, defined by Hadley *et al.* [15] from Hertzian theory as:

$$b = \sqrt{\frac{4\tilde{s}_{11} F R}{\pi}} \qquad (1)$$

where $\tilde{s}_{11}$ is the reciprocal of the plane strain transverse modulus, $\tilde{s}_{11} = s_{11} - s_{13}^2/s_{33} = 1/E_t - \nu_{lt}^2/E_1$, 1 and t represent the transverse direction and 3 and l the fiber direction, F is the force applied per unit length, and R is the fiber radius. In anisotropic fibers where $E_1 \gg E_t$, the plane strain transverse modulus is approximately the fiber transverse modulus, $\tilde{s}_{11} \approx s_{11} = 1/E_t$, so $b(F)$ depends essentially only on transverse modulus in highly anisotropic fibers. Following the Hertzian assumption that the contact area is small relative to the size of the contacting body, $b \ll R$, the boundary conditions in Fig. 2B lead to the force-deflection curve [19]:

$$U_y = \frac{4F\tilde{s}_{11}}{\pi}\left[0.19 + \sinh^{-1}\left(\frac{R}{b}\right)\right] \qquad (2)$$

Using transparent platens to compress sufficiently thick monofilaments would also allow E_t to be determined by fitting experimental data directly to Equation 1 [14, 15, 17].

These analyses are predicated on the assumption of plane strain (or alternately plane stress). Highly anisotropic fibers cannot be sectioned cleanly [14] (cf. [28, 29]), so part of their length cannot be evenly compressed (in contrast to ceramic fibers [8, 9]). Plane strain can be approached by contacting sufficiently long sections of fiber, but as the loaded length decreases, the unloaded tails outside the platens forces the stress state in the fiber to deviate from plane strain (and not approach plane stress), to a three-dimensional stress state, in which stress concentrations at the platen edges cannot be neglected. This means short aspect ratio tests
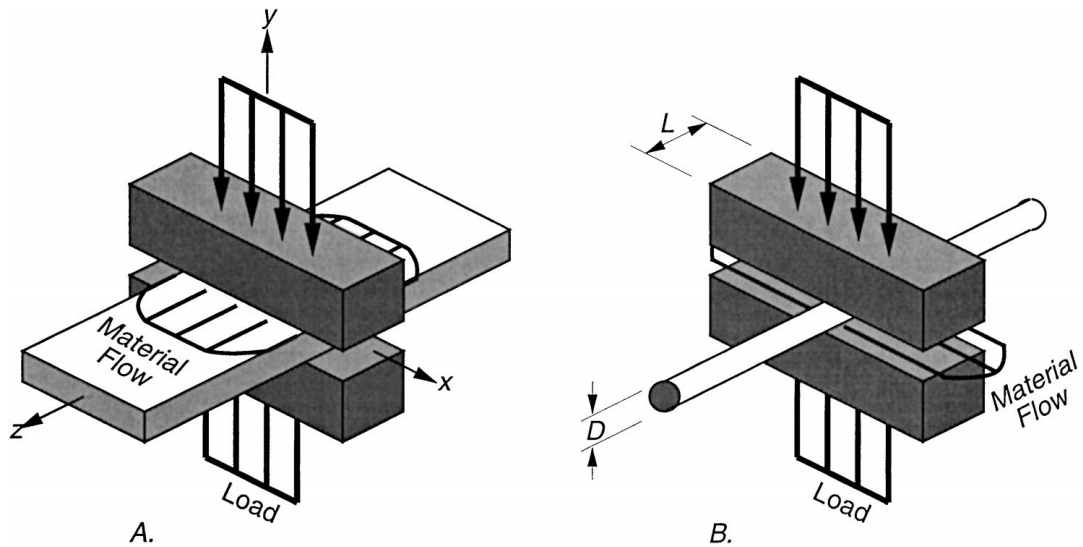
Figure 3 Material flow directions in (A): plane strain compression tests on films, and (B): Plane strain compression tests on highly anisotropic fibers.

are not amenable to classical, two-dimensional analyses, however, they can be analyzed by FE or other, numerical methods.

2.2. Inelastic transverse compression

To understand deformation in SFTCT, it is worthwhile to contrast the plane strain compression of highly anisotropic fibers to the plane strain compression of films (Fig. 3). Film plane strain compression constrains material flow to primarily z. In SFTCT of highly anisotropic fibers, material flow is primarily in x, perpendicular to the fiber axis. Previous investigations [1, 10–12, 14] used long platens ($L/D > 20$), partly to increase experimental forces, but also to ensure that fiber-platen friction prohibited strain in z, since the subsequent analysis assumed plane strain. For highly anisotropic fibers, long platen lengths are unnecessary for this purpose: with typical Poisson ratios, $\nu_{lt} = 0.3$–0.6 [17, 30], and anisotropic ratios, $E_1/E_t \geq 30$, the axial strain resulting from unit transverse strain is $\nu_{tl} = \nu_{lt} E_t/E_1 \approx 0.01$ [3]. Thus, fiber anisotropy alone essentially prevents strain in z, constraining it instead to x.

Transverse yield of polymer fibers has been characterized only qualitatively [1, 12, 14, 18]. The inelastic deformation of PPTA fibers will be discussed in greater detail in a related paper [31].

3. Experimental
3.1. Samples
We tested 1.5 and 6.0 denier KEVLAR 29 continuous filament fibers, corresponding to 12 and 24 μm nominal diameters. 3–6 cm of tows were teased apart and single fibers carefully extracted. Fibers were tested as received, with no additional heat or drying treatment, at $22 \pm 2°$C and 65% RH.

3.2. Transverse compression experiments
SFTCT were performed on a device originally built for plane strain compression testing of thin polymer films [13] (Fig. 4). Motion was provided by a piezoelectric crystal (PZT) (Physik Instrumente P840.60) with a travel of $\approx$50 μm. Force and displacement were transduced by a 50 gmf ($\approx$500 mN) load cell (Transducer Techniques), and an air gap capacitive sensor (Physik Instrumente D-050), respectively. A feedback
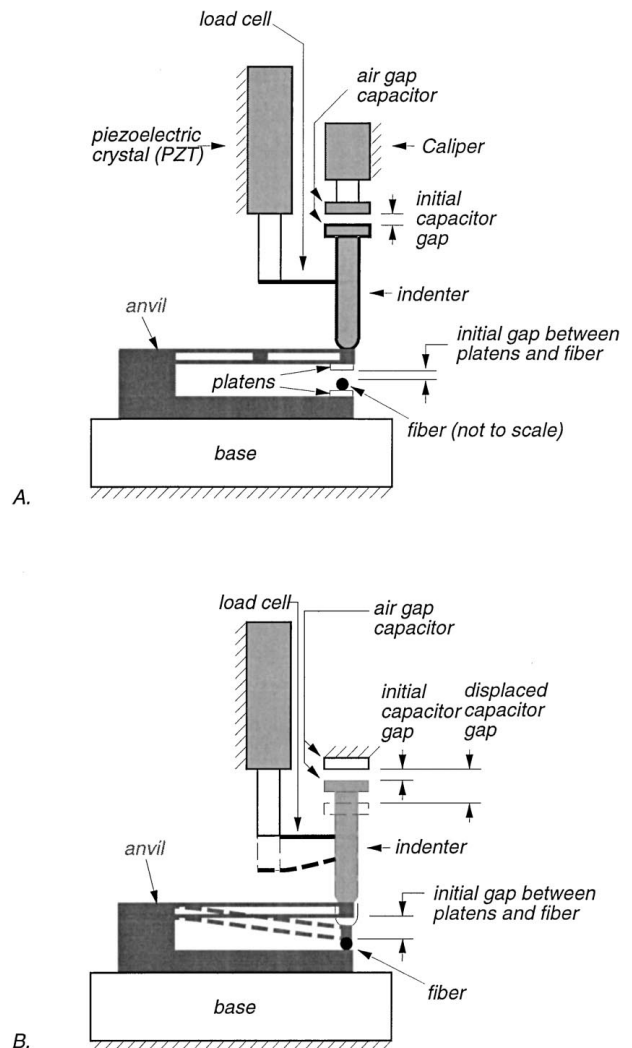
Figure 4 SFTCT device. (A): Initial, (B): deformed during testing.

575
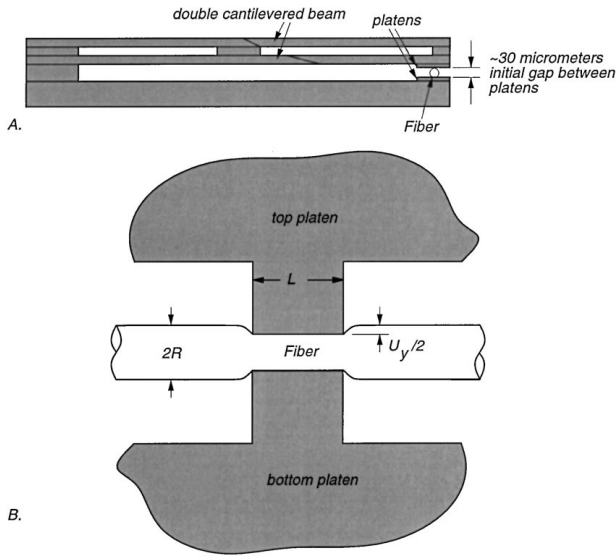
Figure 5 The anvil. (A): Side view, (B): front view, with deformed fiber parallel to plane of paper.

loop between the capacitive sensor and the PZT (Physik Instrumente P864.00) corrected for drift and hysteresis. A P/C controlled PZT displacement signal voltage and recorded force and deflection output. Tests were conducted at constant cross-head speed to a total force of about 400 mN, corresponding to an apparent strain* $e = U_y/D \approx 80\%$ in the smaller fibers, and $e \approx 45\%$ in the larger fibers. Platen design and correcting for machine compliance require further discussion.

3.2.1. Platen design
The platens were machined from a stack of monocrystalline silicon wafers, called the anvil (Fig. 5) [32]. The wafers were machined and fusion bonded under a microscope, insuring the upper and lower platen centers were less than 1 μm offset from each other in z. The anvil contained several pairs of platens, of different lengths, L, between 5 and 75 μm. The platen faces were photo-etched from polished silicon wafers, with an RMS surface roughness less than 2 nm [13]. This is about three orders of magnitude less than the fiber diameter, a necessary criterion for smooth contact. The lower platen faces were photo-etched on a base plate, while the upper platen faces were etched beneath individual, double-cantilevered beams, which insured platen parallelism during deflection (Fig. 4B). Platen face lengths varied within ±10% of nominal lengths.

3.2.2. Machine compliance
Machine compliance was subtracted from the experimental force-deflection data, $F_{exp}(U_{exp})$, by assuming a spring model (Fig. 6) [13]. The bending stiffness of the cantilevered upper platen, k_a, was in parallel with the fiber, and the stiffness of the base, k_b, was in series with the fiber. k_a and k_b were determined for each test by pressing the platens together with no fiber between

---

* The *apparent strain* e is not a strain experienced locally in the fiber, but is a useful measure of deformation.
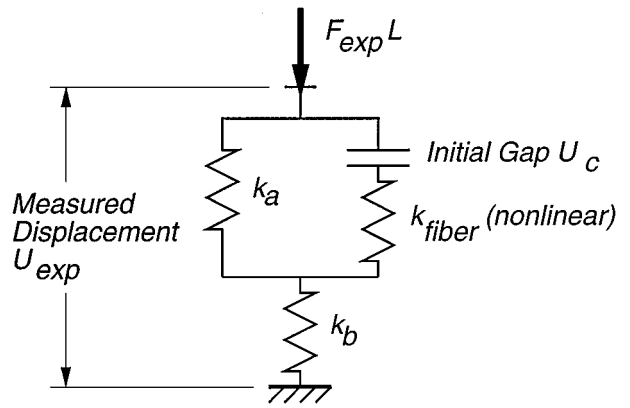
Figure 6 Spring model of SFTCT device used to subtract machine compliance.

the platens. This resulted in a bilinear curve, whose stiffnesses were taken as $k_1 = 1/(1/k_a + 1/k_b)$ before the platens contacted each other at some deflection, U_0, and $k_2 = k_b$ after the platens contacted each other. With k_a and k_b determined for a test, the force per unit length and deflection of the fiber itself, F and U_y, respectively, were calculated from the spring model as:

$$U = U_{exp} \left/ \left[1 + \frac{F_{exp} - F_c}{k_b(U_{exp} - U_c)} \right] \right. \tag{3}$$

$$F = F_{exp} - k_a(U_{exp} - U_c) \left/ \left[1 + \frac{F_{exp} - F_c}{k_b(U_{exp} - U_c)} \right] \right. \tag{4}$$

where U_c and F_c were the displacement and force at contact, respectively. U_c is the distance between the top of the fiber and the upper platen at the beginning of the test, and was determined individually for each test by determining the lowest displacement at which $F_{exp} - k_1 U_{exp}$ was significantly larger than the noise of the data. Fig. 7 shows an example of the experimental and extracted fiber force-deflection curves, starting from the point at which the upper platen first contacted the fiber.

In operation (Fig. 4B), a fiber was placed between a pair of platens of desired length, leaving a 5–15 μm gap between the top of the fiber and the upper platen. The PZT drove a stiff indenter at a constant speed, which pressed the upper, cantilevered platen down, eventually into contact with the fiber at deflection U_c, when fiber compression began. Elastic fiber compression took a few seconds, and the total fiber compression took less than a minute, short enough for viscous effects in the transverse direction of PPTA to be neglected [33].

3.3. Finite element simulation
A three-dimensional FE model was constructed to investigate the effect of specimen aspect ratio on fiber stress state and test force-deflection curve. The model was constructed in ABAQUS/EXPLICIT, using linear elements. The FE model was a right circular cylinder pressed along part of its length by a pair of stiff, parallel platens. The platen edges had a slight fillet, to prevent what would have otherwise been a singularity in the loading. The FE simulation modeled only half
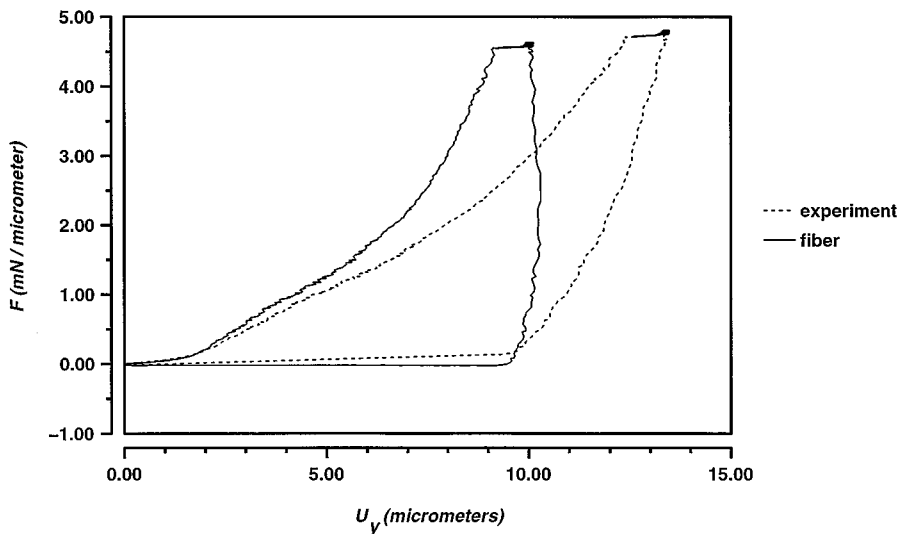
Figure 7 Experimental force-deflection curve, $[U_{exp} - U_c, F_{exp} - F_c]$, and extracted fiber force-deflection curve, $[U_y, F]$. 1.5 denier continuous filament KEVLAR 29.

TABLE I Elastic constants used in finite element simulation of 6.0 denier KEVLAR 29 in SFTCT. Constants assume fiber is transversely isotropic

E_L	80 GPa
E_t	2.2 GPa
G_{lt}	2.2 GPa
ν_{lt}	0.63
ν_{tt}	0.43
R	12 μm

the fiber; for clarity, results in this paper are shown for the entire fiber. To simulate loading, platens were incrementally displaced towards the fiber center, with the resulting contact problem solved at each platen displacment. The test was simulated to $e \approx 5\%$. The fiber was modeled to a length of about 16 fibers diameters outside the platen. Elastic constants used were from experimental results on KEVLAR 29 fibers [11, 34] and composites [30], and are given in Table I.

4. Calculation of transverse properties

Previous researchers [1, 11] have fitted the linear portion of the smoothed derivative of the experimental force-deflection curve, $\partial F/\partial U_y$, to Hertzian contact models (either Equation 2 or analogous equations in [1]), ignoring non-reproducible data at initial contact. We were able to get reproducible initial contact data with KEVLAR 29 filaments, which generally fitted the Hertzian prediction, likely because of greater platen smoothness and shorter loaded length compared to previous studies. Following Jones *et al.* [12], we determined E_t for each test by fitting experimental force-deflection data to Equation 2. R was defined as $2R = U_c - U_0$ for each test. (This generally yielded fiber diameters smaller than published values. This systematic error was accepted because its effect was small relative to the variation in stiffnesses from test-to-test: recalculation with the published fiber diameters instead of the individually, experimentally measured diameters would reduce E_t on average by less than 5%, which is

less than the 95% confidence interval of E_t.) With R known, E_t was determined by nonlinear least squares.

The apparent strain at yield, $e_y = U_{y,\text{yield}}/D$, was determined by eye as part of the E_t fit. Previous studies have used the maximum of the $\partial F/\partial U_y$ curve to define yield, however, that also requires some subjective judgment, as the smoothed derivative does not always have a single peak around the yield point [11]. The work of compression per unit fiber length as a function of deformation, $W(e)$, was calculated as $W(e) = D \int_0^e F dU_y$ by the trapezoidal rule.

5. Results
5.1. SFTCT results
Fig. 8 shows typical force-deflection data for 1.5 denier KEVLAR 29, after correcting for machine compliance, and fitted to Equation 2. The force-deflection curve is upwardly concave during initial, elastic response, as predicted by Equation 2. The tangent stiffness drops and inelastic fiber deformation starts at some deformation, e_y, typically around 5–8%. Fig. 8 demonstrates the variability in our test results: while we found an average transverse stiffness of $E_t \approx 2.4$ GPa, this test had a least-squares fitted stiffness of $E_t = 0.88$ GPa.

Table II gives the average experimental aspect ratio of each, L/D, the effective transverse moduli, E_t, the apparent strain at yield, e_y, and the maximum shear stress at the onset of yield, τ_{max}, as predicted by Hertzian contact analysis. For continuous filaments, the 95% confidence intervals for E_t and e_y are roughly a fifth of the means, reflecting the historical uncertainty of SFTCT [12, 14, 15] that may be an intrinsic characteristic of oriented fibers.

The Hertzian analysis assumes plane strain, an increasingly poor assumption as L/D decreases. Fig. 9 plots E_t versus L/D. E_t appears insensitive to L/D for $L/D \geq 2$, suggesting that above this aspect ratio, the test is reasonably characterized by plane strain models. At lower aspect ratios, the fiber appears to stiffen, a consequence of the increasing importance of edge effects.

TABLE II Transverse moduli, E_t, and apparent yield strain, e_y, of fibers tested in this study, assuming plane strain compression. Plus/minus values indicate the 95% confidence interval

Fiber	Nominal diameter (μm)	Aspect ratio, L/D	Number of tests	E_t (GPa)	e_y (%)	τ_{max} (MPa)
1.5 denier KEVLAR 29	12	7.2	38	2.45 ± 0.40	6.1 ± 1.1	88
6.0 denier KEVLAR 29	24	2.6	20	2.38 ± 0.43	3.9 ± 1.1	64
	24	2.2	35	2.30 ± 0.31	3.3 ± 0.6	
	24	1.2	27	2.85 ± 0.72	2.5 ± 0.4	
	24	0.72	42	3.66 ± 0.24	2.9 ± 0.3	
	24	0.24	38	6.03 ± 0.51	3.3 ± 0.7	
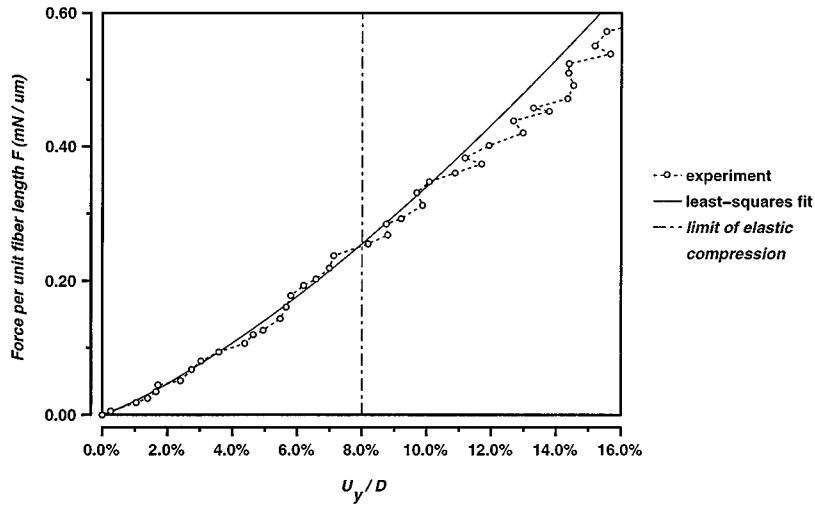
Figure 8 Typical low-deformation SFTCT output.
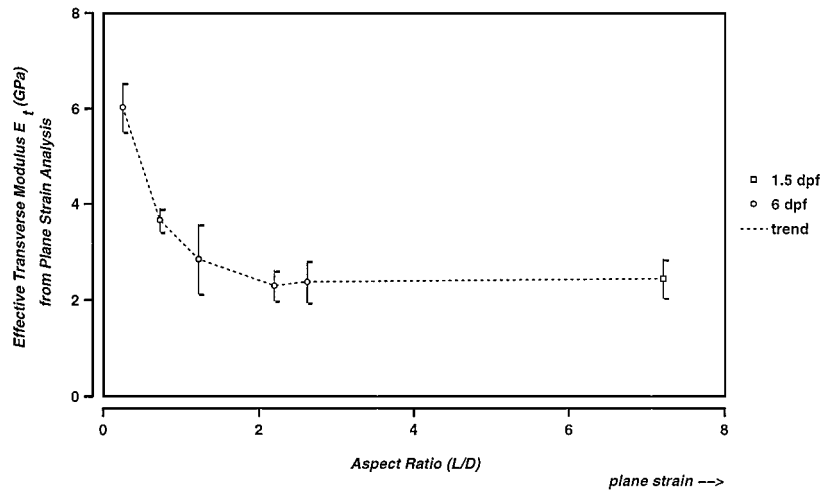
Figure 9 Apparent transverse modulus E_t as a function of aspect ratio of test, for SFTCT of KEVLAR 29 fibers. E_t values all assume plane strain loading. Error bars indicate 95% confidence intervals.

Fig. 10 shows the work per unit length, W, required to compress KEVLAR 29 fibers to $e = 50\%$. W is normalized by denier: since denier is proportional to mean cross-sectional area, this value is proportional to the mean work done per unit volume of fiber compressed. Similar to elastic results, W per denier appears constant for $L/D \geq 2$, and increases with decreasing aspect ratio below $L/D = 2$. The amount of work required to compress fibers to their elastic limit is negligible compared to the amount required to compress fibers to half their initial diameter, a consequence of both the geometric nonlinearity of the test (fibers widen as they flatten), and

more interestingly, indicative of the amount of work required to continue crushing the fibers after they begin to yield.

5.2. FE simulation

Fig. 11 plots FE predictions of the normal stress, σ_y, in a fiber loaded along a short length. There is a stress concentration at the platen edge. The exact stress concentration cannot be accurately predicted by the model; elasticity theory predicts a singularity directly under the platen edge (cf. [35, Article 37]). In actual tests,

Figure 10 Average work per unit length per denier *vs.* apparent strain for KEVLAR 29 fibers in transverse compression at different aspect ratios.

Figure 11 FE predictions for isostress contours for normal stress σ_y of PPTA fiber in SFTCT (platen not shown). $L/D = 4$. Note extent of stress concentration at edge of platen contact.

the platen edge will have some curvature, and the fiber is able to yield locally, both of which reduce the local stress concentration. This modeling limitation does not greatly influence predicted force-deflection curves, which is an integral of the stress distribution. Fig. 12 compares FE predictions of SFTCT force-deflection curves with average experimental results, which have all been normalized to a fiber diameter of 24 μm. Average experimental results at aspect ratios above $L/D = 2$ are in close agreement with FE simulations, and appear independent of L/D. Average experimental results for

the smallest aspect ratio, $L/D = 2.4$, are close to FE predictions for $L/D = 1/4$.

6. Discussion

Fig. 9 suggests SFTCT of highly anisotropic fibers can be reasonably modeled as plane strain when $L/D \geq 2$, allowing direct comparison to tests at much larger aspect ratios in the literature. Table III compares E_t for $L/D \geq 2$ with other SFTCT values for 1.5 denier KEVLAR 29 in the literature. The moduli measured by

Figure 12 Comparison of finite element (FE) and average experimental force-deflection curves for SFTCT of Kevlar 29 at varying aspect ratio L/D. All results scaled to $D = 24$ μm.

TABLE III E_t from SFTCT for 1.5 denier Kevlar 29

Source	E_t (GPa)	e_y (%)	τ_{max} (MPa)
Here	2.45	6.1	88
	2.38	3.9	64
[1]	0.77		47
[11]	1.2–1.4	6–8	41–68
[10]	2.59	$\approx$5	
[12]	2.5		50.2

Kawabata [10] and Jones *et al.* [12] are within the 95% confidence interval of our results. Knoff [11] and Phoenix and Skelton [1] found stiffnesses about a half and a third of ours, respectively. The latter may be attributable to the long length of fibers tested, which as stated above may lead to uneven initial contact, resulting in lower measured stiffness. There is no simple hypothesis to explain the differences between Knoff [11] and Kawabata [10], who used identical test devices, and who fitted their data to equations which differ negligibly. There is more agreement on the apparent transverse yield strain than transverse modulus, with $e_y \approx$ 6–8% for 1.5 denier fibers. and $e_y \approx$ 4% for 6.0 denier fibers.

Results for 6.0 denier Kevlar 29 (Table II) suggest that fiber diameter does not significantly affect transverse stiffness, but does affect transverse strength, in the range of diameters (12–24 μm) tested. The difference in yield points may reflect prior damage from handling, since thicker fibers have a lower yield curvature in bending.

For aspect ratios below $L/D = 2$, the loading is no longer approximately plane strain. The fiber spuriously appears to stiffen as L/D decreases. The apparent failure strain appears unaffected by aspect ratio down to $L/D = 1/4$, suggesting that the fiber failure criterion is independent of the changing stress state. Experimental observations of the effect of aspect ratio on force-deflection curve are verified by FE simulation.

The large anisotropic ratios of highly-oriented fibers do not seem to increase the stress decay rate in SFTCT, as it does in axial fiber testing. Literature [36, 37] suggests stress decay rate is a function of the ratio of normal to shear modulus. In axial testing, it is $\sqrt{E_l/G_{lt}}$. There appears to be no simple description of the stress decay rate in SFTCT, however, experiment suggests it may be dominated by $\sqrt{E_t/G_{lt}}$, which is near unity [2] in PPTA fibers—even smaller than it would be for isotropic materials—therefore requiring a relatively short loaded length to approach plane strain.

PPTA fibers yield in transverse compression, deforming in a ductile manner. High fiber anisotropy forces material to flow essentially perpendicular to the fiber axis. The work required to compress fibers elastically is negligible compared to the amount of work required to continue compression in the yield regime.

PPTA fibers are not truly transversely isotropic, but cylindrically orthotropic [38], and are not homogeneous, but have a radially-dependent gradient of crystalline orientation and perfection [28, 39]. Thus, E_t measured from SFTCT must be considered an *effective* stiffness of the fiber as a structure. The more complicated structure of the actual fiber cross-section will affect the growth of the yield envelope, underscoring the approximation inherent in the FE simulation presented here. The effects of anisotropy and inhomogeneity will be examined in a related paper [31].

7. Conclusions

Single fiber transverse compression tests were performed on Kevlar 29 tests on a novel test device, whose platen designed ensured smooth contact between fibers and the platens. Elastic compression gave reproducible initial contact results, which were fitted directly to Hertzian contact models to determine effective transverse stiffness and apparent strain at yield. There was considerable variation in test results, but the averages, $E_t \approx 2.4$ GPa and $e_y = 6\%$, were similar to results in the literature. Elastic stiffness was independent of fiber diameter; apparent yield strain decreased with increasing diameter.

Both elastic and inelastic compression were independent of loaded fiber length and similar to plane strain results in the literature for $L/D \geq 2$. At lower aspect ratios, deformation outside the loaded fiber length made the fiber spuriously stiff when fitted to planar analyses. Fibers required significant work to continue compression after yield, suggesting a mechanism for energy removal in impact- and cut-resistant applications.

Acknowledgements

References

1. S. L. PHOENIX and J. SKELTON, *Textile Res. J.* **65** (1974) 934.
2. S. B. WARNER, "Fiber Science" (Prentice Hall, Englewood Cliffs, NJ, 1995).
3. S. L. PHOENIX, Technical report N66604-74-C-0318, Naval Underwater Systems Center, Purchase Division, Bldg. 126T, Newport, RI, June 1974.
4. A. E. BOGDANOVICH and C. M. PASTORE, "Mechanics of Textile and Laminated Composites with Applications to Structural Analysis" (Chapman Hall, London, 1996).
5. P. J. F. WRIGHT, *Magazine Concrete Res.* **20** (1995) 87.
6. G. HONDROS, *Australian J. Appl. Sci.* **10** (1959) 243.
7. K. G. KRIEDER and K. M. PREWO, "Composite Materials: Testing and Design (Second Conference)" (Philadelphia, PA, 1972. ASTM STP 497). p. 539.
8. A. R. BUNSELL and T. T. NGUYEN, *Fibre Sci. Tech.* **13** (1980) p. 363.
9. J. I. ELDRIDGE, J. P. WIENING, T. S. DAVISON and M.-J. PINDERA, *J. Amer. Ceramics Soc.* **76** (1993) 3151.
10. S. KAWABATA, *J. Textile Inst.* **81** (1990) 433.
11. W. F. KNOFF, in Proceedings of the 21st Textile Research Symposium (Fuji Educational Training Center, Susono City, Shizuoka, Japan, 7–9 August 1992) p. 5.
12. M.-C. G. JONES, E. LARA-CURZIO, A. KOPPER and D. C. MARTIN, *J. Mater. Sci.* **32** (1997) 2855.
13. L. LIN, in Proceedings of the ASME International Mechanical Engineering Annual Conference, San Francisco, CA, edited by Mary C. Boyce (ASME, New York, NY 1995) p. 117.
14. T. KOTANI, J. SWEENEY and I. M. WARD, *J. Mater. Sci.* **29** (1994) 5551.
15. D. W. HADLEY, I. M. WARD and J. WARD, *Proc. Royal Soc. A* **285** (1965) 275.
16. P. R. PINNOCK, I. M. WARD and J. M. WOLFE, *ibid. A* **291** (1965) 267.
17. D. W. HADLEY, P. R. PINNOCK and I. M. WARD, *J. Mater. Sci.* **4** (1969) 152.
18. S. K. BATRA and S. NURUZZAMAN, *J. Polym. Sci. Polym. Phys. Ed.* **13** (1975) 369.
19. S. A. JAWAD and I. M. WARD, *J. Mater. Sci.* **13** (1978) 1381.
20. S. MORRIS, *J. Textile Inst.* **59** (1968) 536.
21. J. N. SINGLETARY, PhD thesis, North Carolina State University, Raleigh, NC (1998).
22. R. BEECHING and W. NICHOLLS, in "The Institute of Mechanical Engineers Proceedings" (The Institution of Mechanical Engineers, Storey's Gate, St. James Park, London, January 1948) p. 317.
23. E. MCEWEN, *ibid.* p. 324.
24. *Idem.*, *Philosophical Mag.* **40** (1949) 454.
25. H. OLESIAK and A. P. WILCZYŃSKI, *Mechanika Teoretyczna* **3** (1975) 353.
26. B. L. DHOOPAR and P. K. SINHA, *Fibre Sci. Tech.* **19** (1983) 179.
27. T. S. DAVISON, H. N. G. WADLEY and M.-J. PINDERA *Composites Eng.* **4** (1994) 995.
28. M. G. DOBB and R. M. ROBSON, *J. Mater. Sci.* **25** (1990) 459.
29. M. G. DOBB, C. R. PARK and R. M. ROBSON, *ibid.* **27** (1992) 3876.
30. S. KAWABATA, M. SERA, T. KOTANI, K. KATSUMA, M. NIWA and C. XIAOXIN, Technical report, Department of Polymer Chemistry, Kyoto University, Kyoto 606, Japan, April 1993.
31. J. SINGLETARY, H. DAVIS, Y. SONG, M. K. RAMASUBRAMANIAN and W. KNOFF, *J. Mater. Sci.* **35** (2000) 583.
32. L. LIN and M. H. JOHNSON, U.S. Patent no. 5517860, May 21 (1996).
33. S. KAWABATA and K. KATSUMA, in Proceedings of the 21st Textile Research Symposium (Fuji Educational Training Center, Susono City, Shizuoka, Japan, 7–9 August 1992) p. 1.
34. W. F. KNOFF, *J. Mater. Sci.* **22** (1987) 1024.
35. S. P. TIMOSHENKO and J. N. GOODIER, "Theory of Elasticity, 3rd ed" (McGraw-Hill, New York, 1970).
36. C. O. HORGAN, *Appl. Mech. Reviews* **42** (1989) 295.
37. *Idem.*, *ibid.* **49** (1996) S101. part 2.
38. H. R. BLADES, U.S. Patent no. 3869429, March 4 (1975).
39. R. J. YOUNG, D. LU, J. DAY, W. F. KNOFF and H. A. DAVIS, *J. Mater. Sci.* **27** (1992) 5431.